IOPscience iopscience.iop.org

Home Search Collections Journals About Contact us My IOPscience

Finding best-fit polyhedral rotations with geometric algebra

This article has been downloaded from IOPscience. Please scroll down to see the full text article.

2002 J. Phys.: Condens. Matter 14 4567

(http://iopscience.iop.org/0953-8984/14/17/327)

View the table of contents for this issue, or go to the journal homepage for more

Download details:
IP Address: 171.66.16.104
The article was downloaded on 18/05/2010 at 06:35

Please note that terms and conditions apply.

INSTITUTE OF PHYSICS PUBLISHING JOURNAL OF PHYSICS: CONDENSED MATTER

J. Phys.: Condens. Matter **14** (2002) 4567–4584 PII: S0953-8984(02)31520-0

Finding best-fit polyhedral rotations with geometric algebra

Stephen A Wells, Martin T Dove and Matthew G Tucker

Mineral Physics Group, Department of Earth Sciences, University of Cambridge, Downing Street, Cambridge CB2 3EQ, UK

Received 4 December 2001
Published 18 April 2002
Online at stacks.iop.org/JPhysCM/14/4567

Abstract

There are many minerals whose structure is well described as a framework of linked SiO_4 tetrahedra. Since the energy cost of stretching the Si–O bond is much greater than the cost of changing the bridging Si–O–Si bond angle, these structures may to a first approximation be analysed using the rigid-unit picture, in which the polyhedra are treated as completely rigid. In order to compare the predictions of rigid-unit theory with the results of other forms of simulation, we wish to determine how well a given set of atomic motions can be described in terms of rigid-unit motion. We present a set of techniques for finding the polyhedral rotations that most closely fit a given set of atomic motions, and for quantifying the residual distortion of the polyhedra. The formalism of geometric (Clifford) algebra proved very convenient for handling arbitrary rotations, and we use this formalism in our rotor-fitting analysis.

(Some figures in this article are in colour only in the electronic version)

1. Introduction

Many materials have crystal structures that can be described as frameworks of linked polyhedral groups of atoms. Examples include the perovskites such as $SrTiO_3$, which contains corner-linked TiO_6 octahedra, zeolites and other silicates with networks of corner-linked SiO_4 and AlO_4 tetrahedra, and ceramics with negative thermal expansion such as ZrW_2O_8, which contains corner-linked ZrO_6 octahedra and WO_4 tetrahedra. These materials have a wide range of properties, such as the existence of phase transitions [1] and anomalous thermal expansion [2, 3], that can be explained by models in which the polyhedra are effectively rigid and in which the framework is allowed to flex without high cost in energy. This approach has been quantified by the 'rigid-unit-mode' (RUM) model, in which the flexibility of the network is interpreted in terms of low-energy phonons in which the polyhedra move as rigid units [1,4]. These phonons are what have been called RUMs. Using methods reviewed below, it has been possible to show that most framework materials do not have large numbers of RUMs. However, since RUMs have very low frequencies their amplitudes can be large and so the RUMs that do

 © 2002 IOP Publishing Ltd Printed in the UK

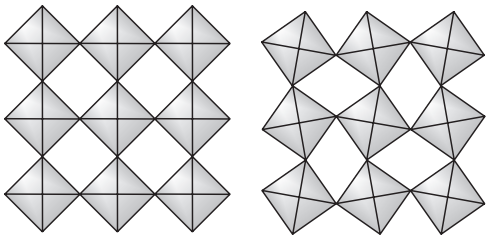

Figure 1. The octahedral rotation mode in the perovskite structure is an example of a RUM.

exist play a significant part in phenomena such as displacive phase transitions, zeolite catalysis, and negative thermal expansion.

The RUM model has been formulated in terms of phonons and the distribution of RUM phonons in reciprocal space [1,4]. Some progress towards developing the model in the variables of real space has been made by projecting a set of RUM eigenvectors onto a supercell structure in order to quantify the localized flexibility of zeolite networks. In this paper we develop the mathematical tools to facilitate the analysis of RUM deformations in real-space atomic configurations. These are based on the technique of 'geometric algebra' (GA) [6]. We illustrate the tools using two example studies. The first is the analysis of large configurations of disordered crystalline phases of the silica polymorphs in order to obtain a quantitative measure of the contribution of the RUMs to the overall atomic motions. The second is an analysis of local deformation of framework structures due to an atomic substitution on a tetrahedral site.

2. Rigid-unit-mode model

2.1. Rigid-unit modes

We noted above that the RUMs are phonon modes in which the polyhedral groups of atoms move as rigid units. In the simplest visualization of these motions, we can treat the polyhedra as rigid units with a nominal high value of a single coefficient of stiffness for deformation, and with no other force constants in the system. The RUMs will therefore be the phonons with zero frequency. Other phonons will have values of their frequencies that are determined by the extent to which the polyhedra are distorted. The simplest example of a RUM is the octahedral rotation mode in the perovskite structure, as shown in figure 1. In practice there is a wide range of force constants for interactions between polyhedra, as well as a more complicated set of interactions that describe the deformations of the polyhedra. Nevertheless, this latter set of force constants will have values that are higher than other force constants in the materials, and the RUMs will have low frequencies. Typically it is found that the RUM frequencies lie between 0 and 1 THz [5]. In materials that undergo displacive phase transitions, more RUMs are found in the higher-symmetry high-temperature phases [1]. In many cases, these phases appear to contain considerable orientational disorder of the polyhedra. The structures of these phases can be interpreted in terms of the dynamic superposition of RUMs across a wide range of wavevectors [7]. In many cases, the soft modes for displacive phase transitions have been identified as RUMs [1]. The case of quartz is one in which this has been documented in some detail [1, 8].

The theoretical task is to identify the set of phonon modes that are RUMs. This task involves identifying both the wavevectors of the RUMs and the RUM eigenvectors. We use a molecular dynamics approach within the 'split-atom' approximation, as described below [4,9].

For many framework structures we typically find that the RUMs lie on surfaces of wavevectors in reciprocal space. Often these are flat surfaces that lie on special planes, including planes that pass through $\boldsymbol{k} = 0, 0, 0$, and planes that lie on the surfaces of the Brillouin zone. However, we have also found that for some materials the RUMs lie on exotic curved surfaces in reciprocal space; the reason for this is not known [5]. We have also identified the existence of RUMs in silica and silicate glasses, for which the reciprocal-space analysis is of less relevance [10, 11].

2.2. Split-atom approach

The split-atom method [4] provides a simple representation of a framework structure that facilitates the use of standard molecular lattice dynamics methods for the analysis of potential RUM distortions. The idea is to replace atoms shared between two polyhedra by two atoms, each assigned to one of the two linked polyhedra. These two atoms are the split atoms. The equilibrium separation of the two split atoms is zero, and this is maintained by a fictitious spring of zero equilibrium length operating between the two split atoms. The array of polyhedra with split atoms on the vertices can be relatively easily analysed using molecular lattice dynamics, in which each polyhedron is treated as a perfectly rigid object with six degrees of freedom. The only force constant in the calculation is the stiffness of the spring between two split atoms. In fact this spring represents to first order the forces associated with the distortions of the polyhedra, and the spring force constant can be tuned so that the spread of phonon frequencies matches the experimental spread (since the highest phonon frequencies are those associated with modes of deformation of the polyhedra). The dynamical matrix for this system can be set up using standard methods.

The molecular lattice dynamics calculation can be performed for any chosen wavevector. For each wavevector, any RUM will be calculated to have zero frequency. The atomic motions associated with any RUM can be obtained from the corresponding mode eigenvector.

2.3. Atomistic simulations

There are a wide variety of simulation tools that can be used to provide configurations of displaced atoms under various different conditions which can then be analysed in terms of RUM deformations. In this paper we study two different types of atomic configuration, which we generate using two specific techniques. The first is the reverse Monte Carlo (RMC) method [12, 13]. This involves generating configurations of atoms that give best agreement with experimental data, which in our case are data from neutron total-scattering experiments. Similar configurations can also be obtained from molecular dynamics or Monte Carlo simulations with interatomic potentials, but for our purposes the use of the RMC method ensures that we have configurations that are truly consistent with experimental data and are not influenced by the details of model interatomic potentials. The methodology is described in more detail elsewhere [12–14]. For the present work, we use a series of configurations of quartz over a wide range of temperatures encompassing the α–β phase transition [15], and use the GA tools to analyse how fluctuations in the structure can be described quantitatively in terms of rigid-body rotations of the SiO_4 tetrahedra and small deformations of the tetrahedra.

The second type of atomic configuration that we study in this paper is concerned with the relaxation of framework crystal structures around defect sites. The structures of many silicates consist of networks of linked SiO_4 and AlO_4 tetrahedra, and frequently it is found that the Al and Si cations are disordered across the different tetrahedral sites. A lot of research has been concerned with understanding the ordering interactions, which are primarily determined by the strains associated with the differences in sizes of the Si and Al cations [16, 17]. An interesting

issue is how the strain can be propagated across the tetrahedral framework because it is possible, in principle, for the strain to be screened by rotations of the tetrahedra. In this paper we use a single demonstration calculation to show the potential of the GA approach for addressing this issue. In this case, we generate the atomic configuration using the Mott–Littleton method. We start with a purely siliceous framework and incorporate a single Al cation within one of the tetrahedral sites as a charged defect. For this work we use the interatomic shell-model potentials described by Winkler *et al* [18]. The Mott–Littleton calculations were performed within the GULP lattice energy program [19].

2.4. Bridging the gap

The RUM and the split-atom approach allow us to identify RUMs according to their wavevector. However, this approach does not give us the actual atomic positions and bond lengths. Atomistic simulations, on the other hand, provide information on atomic positions and bond lengths but have no connection to the RUM. It would obviously be useful to bridge this gap and quantify how closely the rigid-unit approach matches actual atomic motions.

In this paper we present a set of equations for determining how closely a given set of atomic motions can be matched using rigid-unit motions only, and for quantifying the residual distortion of the polyhedra. This allows us to determine for the first time what proportion of the atomic motions in a framework structure can be accounted for by rigid-unit motion.

3. Mathematical approach

We have used the language of GA, as it gives a very convenient form for handling general rotations. There is no need to go into great depth on the subject of GA here, so we shall simply present the axioms and some examples in the appendix. More information on GA can be found in the literature [6, 20, 23] and online [24].

3.1. Equations of a general rotation

Our equations are written here in terms of a three-dimensional set of orthonormal basis vectors e_i, where e_1 is the unit vector in the $\hat{x}$ direction and so on. The rotor operator R, which rotates a vector by the operation $x \rightarrow x' = Rx\tilde{R}$, is defined in the appendix. R is usually written in either an exponential form: $R = \mathrm{e}^{-\hat{B}\phi/2}$, or a trigonometric form: $R = \cos(\phi/2) - \hat{B}\sin(\phi/2)$. In this form $\hat{B}$ is a unit bivector describing the plane of the rotation.

In this work we have found it convenient to use instead the following algebraic form:

$$R = X - \tfrac{1}{2}(B_x e_2 e_3 + B_y e_3 e_1 + B_z e_1 e_2) = X - B/2. \tag{1}$$

In this form the $B_n e_j e_k$ terms form a bivector B, defining the plane of the rotation. Comparison with the trigonometric form gives the modulus of B as

$$|B| = \sqrt{(B_x^2 + B_y^2 + B_z^2)} = 2\sin\left(\frac{\phi}{2}\right), \tag{2}$$

so that for small angles $|B| \simeq \phi$.

The term X is equal to $\cos(\phi/2)$ and is given by

$$X = \sqrt{(1 - \tfrac{1}{4}(B_x^2 + B_y^2 + B_z^2))}. \tag{3}$$

The case $B = 0$ is the identity operation; $R(0) = 1$. The rotor form has this advantage over Euler angles, that there is no coordinate singularity at the origin.

Table 1. Coefficients c_{ij} in equation (7).

Rotation	c_{i1}	c_{i2}	c_{i3}
$Re_1\tilde{R}$	$\left(1-\frac{(B_y^2+B_z^2)}{2}\right)$	$\left(XB_z+\frac{B_xB_y}{2}\right)$	$\left(-XB_y+\frac{B_xB_z}{2}\right)$
$Re_2\tilde{R}$	$\left(-XB_z+\frac{B_xB_y}{2}\right)$	$\left(1-\frac{B_x^2+B_z^2}{2}\right)$	$\left(XB_x+\frac{B_yB_z}{2}\right)$
$Re_3\tilde{R}$	$\left(XB_y+\frac{B_xB_z}{2}\right)$	$\left(-XB_x+\frac{B_yB_z}{2}\right)$	$\left(1-\frac{B_x^2+B_y^2}{2}\right)$

3.1.1. Comparison with the axial-vector form. Since vector algebra is far more widely known than GA, it is useful to be able to convert between the rotor form and a conventional axis and angle. As we have seen, the size of the rotation angle ϕ is given by

$$\phi = 2\arcsin\left(\frac{|B|}{2}\right). \tag{4}$$

The axis of the rotation is given by a unit vector $\hat{b} = b_1e_1 + b_2e_2 + b_3e_3$, whose components b_i are found as follows:

$$\sum_i b_i^2 = 1; \tag{5}$$

$$b_1{:}b_2{:}b_3 = B_x{:}B_y{:}B_z. \tag{6}$$

So for example a bivector whose only non-zero component is B_x describes a rotation in the e_2e_3-plane, or equivalently a rotation about the x-axis; a rotation with $B_x = B_y = B_z$ is a rotation about the [111] direction, and so on. Not only are the B_n convenient parameters for calculation, but also it is easy to visualize their meaning.

3.2. Rotation of basis vectors

We can write the effect of an arbitrary rotation in terms of its effect on the basis vectors as a function of the terms B_n given above, treating the B_n as the parameters of the rotation. In each case we have an equation of the form

$$Re_i\tilde{R} = c_{i1}e_1 + c_{i2}e_2 + c_{i3}e_3, \tag{7}$$

where the coefficients c_{ij} are shown in table 1.

4. Technique

Since we know the effect of a rotation on the basis vectors, we know its effect on any arbitrary vector. We can now make use of this in order to identify the rotational motions of structural polyhedra which, according to the RUM, we expect to find in framework mineral structures.

4.1. Fitting a rotation

To perform the calculation we make use of the bond vectors within each polyhedron. Let us suppose that we have two slightly different forms of the same structure. Let us consider the structure bond by bond. For each bond we have a vector from the central atom p to an atom q at a vertex of the polyhedron; for one form of the structure let us call this vector PQ, for

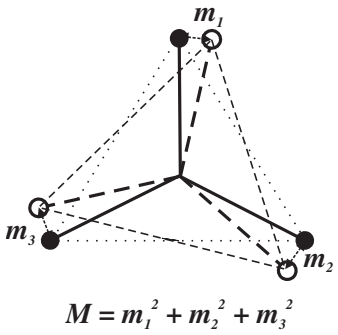

Figure 2. The best-fit rotation is that which minimizes the mismatch value M.

Table 2. The coefficients d_{ij} in equation (8).

E_{qi}	d_{i1}	d_{i2}	d_{i3}	
E_{q1}	$\left(1-\frac{B_y^2+B_z^2}{2}\right)$	$\left(-XB_z+\frac{B_xB_y}{2}\right)$	$\left(XB_y+\frac{B_xB_z}{2}\right)$	$-PQ'_1$
E_{q2}	$\left(XB_z+\frac{B_xB_y}{2}\right)$	$\left(1-\frac{B_x^2+B_z^2}{2}\right)$	$\left(-XB_x+\frac{B_yB_z}{2}\right)$	$-PQ'_2$
E_{q3}	$\left(-XB_y+\frac{B_xB_z}{2}\right)$	$\left(XB_x+\frac{B_yB_z}{2}\right)$	$\left(1-\frac{B_x^2+B_y^2}{2}\right)$	$-PQ'_3$

the other form PQ'. For example, PQ and PQ' might be snapshots of the dynamic disorder in the structure at two different times. Our assumption, from the rigid-unit picture, is that there exists a rotation which takes PQ very close to PQ'. This is illustrated in figure 2. We can also compare the polyhedra in a real structure PQ' to those in an idealized structure PQ with perfectly regular tetrahedra, so as to quantify the distortion of the polyhedra.

4.2. Mismatch equation

We can write down a vector $PQ''(PQ, B)$, representing the vector PQ after the rotation defined by B; this allows us to write a mismatch vector E, given by $E_q = PQ'' - PQ'$. Minimizing this mismatch with respect to the parameters B_n will give the rotation which best fits PQ onto PQ'.

Writing PQ in components as $PQ = PQ_1e_1 + PQ_2e_2 + PQ_3e_3$, we can apply a rotation to PQ using equation (7). The vector E_q can now be written in components as $E_q = E_{q1}e_1 + E_{q2}e_2 + E_{q3}e_3$, which can be written in terms of (PQ, PQ', B):

$$E_{qi} = d_{i1}PQ_1 + d_{i2}PQ_2 + d_{i3}PQ_3 - PQ'_i. \tag{8}$$

The coefficients d_{ij} are shown in table 2.

In order to find a rotation which best fits PQ onto PQ', we also need the derivatives of the E_{qi} with respect to the B_n. Let us note that $X = \sqrt{1-\frac{1}{4}(B_x^2+B_y^2+B_z^2)}$, so $\partial X/\partial B_n = -B_n/(4X)$. The derivatives can be given in the form

$$\frac{\partial E_{qi}}{\partial B_n} = a_{in1}PQ_1 + a_{in2}PQ_2 + a_{in3}PQ_3. \tag{9}$$

The coefficients a_{inj} are shown in table 3.

Table 3. The coefficients a_{inj} in equation (9).

$E_q i$	$\partial/\partial B_n$	a_{in1}	a_{in2}	a_{in3}
E_{q1}	$\partial/\partial B_x$	0	$\left(\frac{B_x B_z}{4X} + \frac{B_y}{2}\right)$	$\left(-\frac{B_x B_y}{4X} + \frac{B_z}{2}\right)$
E_{q1}	$\partial/\partial B_y$	$(-B_y)$	$\left(\frac{B_y B_z}{4X} + \frac{B_x}{2}\right)$	$\left(X - \frac{B_y^2}{4X}\right)$
E_{q1}	$\partial/\partial B_z$	$(-B_z)$	$\left(-X + \frac{B_z^2}{4X}\right)$	$\left(-\frac{B_y B_z}{4X} + \frac{B_x}{2}\right)$
E_{q2}	$\partial/\partial B_x$	$\left(-\frac{B_x B_z}{4X} + \frac{B_y}{2}\right)$	$(-B_x)$	$\left(-X + \frac{B_x^2}{4X}\right)$
E_{q2}	$\partial/\partial B_y$	$\left(-\frac{B_y B_z}{4X} + \frac{B_x}{2}\right)$	0	$\left(\frac{B_x B_y}{4X} + \frac{B_z}{2}\right)$
E_{q2}	$\partial/\partial B_z$	$\left(X - \frac{B_z^2}{4X}\right)$	$(-B_z)$	$\left(\frac{B_x B_z}{4X} + \frac{B_y}{2}\right)$
E_{q3}	$\partial/\partial B_x$	$\left(\frac{B_x B_y}{4X} + \frac{B_z}{2}\right)$	$\left(X - \frac{B_x^2}{4X}\right)$	$(-B_x)$
E_{q3}	$\partial/\partial B_y$	$\left(-X + \frac{B_y^2}{4X}\right)$	$\left(-\frac{B_x B_y}{4X} + \frac{B_z}{2}\right)$	$(-B_y)$
E_{q3}	$\partial/\partial B_z$	$\left(\frac{B_y B_z}{4X} + \frac{B_x}{2}\right)$	$\left(-\frac{B_x B_z}{4X} + \frac{B_y}{2}\right)$	0

4.3. Minimization by steepest descent

We define a mismatch score M by summing the squares of the mismatch vectors E_q over all the bonds in a polyhedron:

$$M = \sum_q \sum_{i=1}^{3} E_{qi}^2. \tag{10}$$

Usually $q = 4$ as we are often dealing with SiO_4 tetrahedra.

We can take M as a function over a vector space whose basis is B_n; since we have the partial derivatives 9, we know not only M but also ∇M:

$$(\nabla M)_n = \sum_q \sum_{i=1}^{3} 2E_{qi} \frac{\partial E_{qi}}{\partial B_n}. \tag{11}$$

To find the minimum of M we use the method of steepest descents, starting from $B = 0$ and taking steps in the direction of $-\nabla M$ until $|\nabla M|$ is sufficiently close to zero to be considered a minimum. B is the best-fit rotation for the polyhedron and the value of M at $B_{\min}$ represents the residual distortion of the polyhedron.

If the bond lengths $l_{PQ}, l_{PQ'}$ differ, then a part of the residual distortion can be attributed to a bond-stretching term. The remainder of the distortion is due to flexing of the tetrahedral angles. So long as the flexions are small then the bond-stretching and bond-angle-bending displacements of the atom Q are approximately orthogonal to each other, so we may divide the residual distortion $E_{q,\text{after}}^2$ into bending and stretching terms, thus: $E_{q,\text{after}}^2 = m_{\text{bend}}^2 + m_{\text{stretch}}^2$. This is illustrated in figure 3.

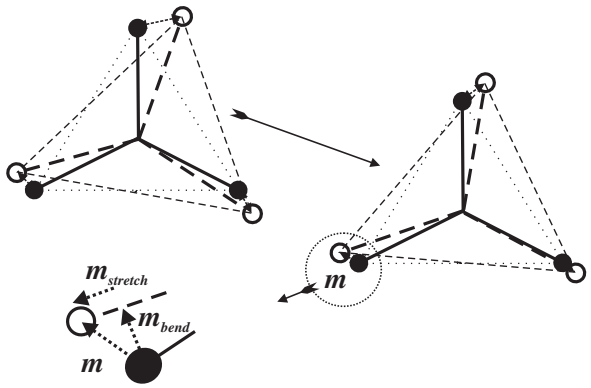

Figure 3. Where both rotation and distortion are present, there will be some residual mismatch, which can be divided into bending and stretching terms.

4.4. Programming routines

The program to carry out this minimization was written in Fortran90. Modules containing functions for equations (8) and (9) and a subroutine for the steepest-descent algorithm are available from www.esc.cam.ac.uk/minsci/downloads.

5. Case studies

5.1. Phase transitions and dynamic disorder

We noted in the introduction that many high-temperature phases appear to have orientational disorder of the polyhedra. One example is β-cristobalite, which has a face-centred cubic structure. Crystallographic analysis has the average positions of neighbouring Si–O–Si atoms in straight linkages. However, in most silicates this linkage has an angle of around 145°. Moreover, the thermal displacement parameters suggest considerable transverse motions of the O atoms, and this has led to the understanding that there is considerable disorder of this phase with large-amplitude motions of the atoms as they seek to avoid forming linear Si–O–Si linkages. Initially it was thought that the structure of this phase could be explained through the formation of small domains of the low-temperature phase or of other ordered phases, but recent work has shown that there is considerable dynamic disorder arising from fluctuations of atomic motions with a wide range of wavevectors [25, 26]. This is consistent with the RUM interpretation in which RUMs across a wide range of wavevectors cause large-amplitude rotations of the tetrahedra. Support for the RUM interpretation has come from molecular dynamics simulations [27], RMC analysis of neutron total-scattering data [28], and inelastic neutron scattering measurements.

The important component of the RUM theory of disordered crystalline framework structures that has yet to be properly quantified is the fraction of the atomic motions that are associated with the RUMs. Although the RUM model highlights the rigid-body motions of the polyhedra, the vast majority of phonons give some deformations of the polyhedra, and we expect to see deformation modes riding on the RUM excitations.

To quantify the extent of the RUM contribution to the atomic motions in disordered phases, we have used large configurations of tetrahedra in silica polymorphs constructed by RMC modelling from neutron total-scattering data. The experimental data and RMC analysis

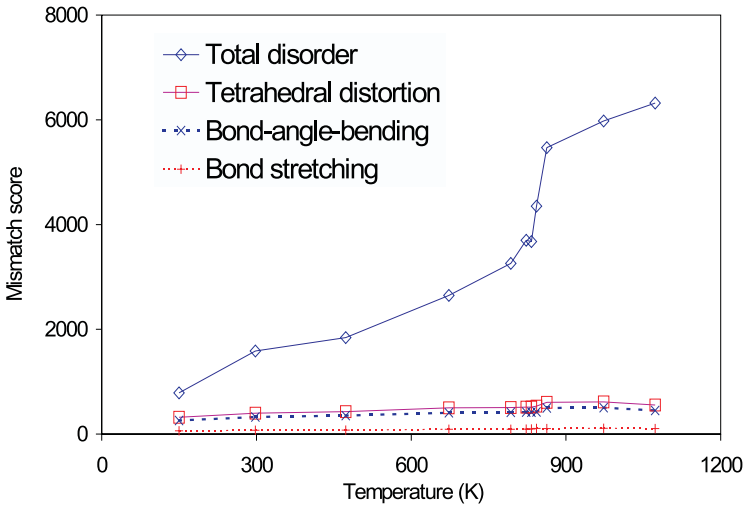

Figure 4. The dynamic disorder in quartz is largely accounted for by rigid-unit motions of the tetrahedra. The difference between the total disorder and the tetrahedral distortion is due to rigid-unit motion. The horizontal axis gives temperature in kelvins; the vertical axis gives mismatch score M in Å^2 summed over 24 000 bond vectors in 6000 polyhedra.

has been described in detail in a number of papers. The essential point here is that the RMC method has been used to generate atomic configurations that have a good consistency with experimental data. It should be noted that the experimental data were collected to a high value of the scattering vector, so there is a good resolution on the atomic positions in real space. The RMC method takes account of the pair distribution function, the overall neutron scattering intensity, and the intensities of the Bragg peaks. As a result, the RMC configurations will capture both the long- and short-range order seen in experiments. The RMC configurations also contained constraints on the bonding in order to avoid the formation of spurious defect states that may arise through the statistical nature of the RMC algorithms.

Two configurations were generated from the scattering data at each temperature value. Both configurations started with the same initial configuration, but the stochastic nature of the RMC algorithms means that the two configurations differed slightly from each other. We treat the two configurations as two snapshots of the dynamic disorder in quartz, and apply our rotor-fitting algorithms, taking the bond vectors PQ from one configuration and PQ' from the other. The initial mismatch score M_{before} before fitting a rotation gives a measure of the total disorder, while the residual mismatch M_{after} after fitting a rotation represents actual tetrahedral distortion; the difference between the two is attributable to rigid-unit motion of the polyhedra. These data are presented in the figure 4.

We note first that the actual tetrahedral distortion is much less than the total disorder. The large difference between the two indicates the contribution of RUMs to the dynamic disorder. Figure 5 gives the RUM contribution as a percentage of the total disorder; this contribution rises from 60 to 70% at low temperature to almost 90% just below the phase transition, and increases above 90% in the β-phase. The amplitude of the RUMs increases with temperature much faster than the amplitude of the non-RUM disorder.

The α–β phase transition is clearly visible in the dynamic disorder, which drops dramatically as the temperature falls below the transition temperature. This is almost entirely due to the effect of the phase transition on the RUMs, as the tetrahedral distortion is almost

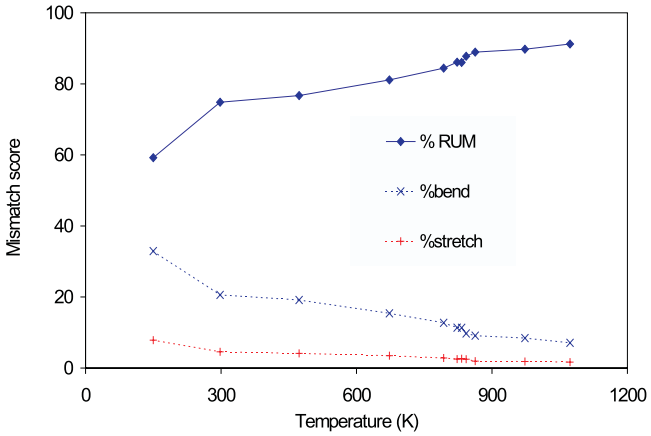

Figure 5. The proportion of the dynamic disorder accounted for by rigid-unit motions of the polyhedra increases with temperature, exceeding 90% in the high-symmetry β-phase. The horizontal axis gives temperature in kelvins. Proportions are given as percentages of the total dynamic disorder at that temperature.

insensitive to the phase transition. There exist phonon modes which are RUMs in the high-symmetry β-phase but become ordinary phonon modes involving tetrahedral distortion in the low-symmetry α-phase. This change is accompanied by a dramatic decrease in amplitude as the frequency of the mode increases from the very low RUM frequency to the frequency of an ordinary phonon mode. We attribute the changes in dynamic disorder with temperature to the effects of the symmetry change on the RUM phonons. The behaviour of the mode frequencies as a function of the order parameter will be discussed elsewhere.

The tetrahedral distortion can be further divided into the terms due to variation in bond lengths and due to bending of the O–Si–O bond angle. It is clear that the distortion is primarily due to bond bending, with a much smaller bond-stretching component. The nature of the distortions does not appear to change over the temperature range of the study.

5.2. Defect accommodation

Many framework structures have more than one type of cation in the polyhedral sites. For example, many silicate minerals and zeolites have a mixture of AlO_4 and SiO_4 tetrahedra. The Si^{4+} and Al^{3+} cations differ in size, and this gives rise to straining of the network when the arrangement of cations does not match. The popular expression of this effect is the so-called 'Al-avoidance rule', which states the observation that Al cations tend to avoid forming nearest-neighbour pairs in framework silicates. The essential point of this rule is that there is a strain-induced tendency to maximize the number of Si–O–Al linkages in order to give the best fitting of the different-sized cations and thereby to reduce the overall strain on the network. It is of interest to understand how the strain propagates through the network. In particular, the strain may be accommodated by RUM-like rotations of the tetrahedra to minimize the size mismatch. We have applied our GA approach to quantify the relaxation of a silica network around a tetrahedral Al^{3+} substitutional defect. This case study is intended as a proof of principle; in a forthcoming paper we shall address the phenomenon of Al avoidance in terms of the response of the structure to pairs of defects.

The basic configurations have been constructed using the Mott–Littleton method for calculating defect energies, as coded into the general modelling program GULP. This approach

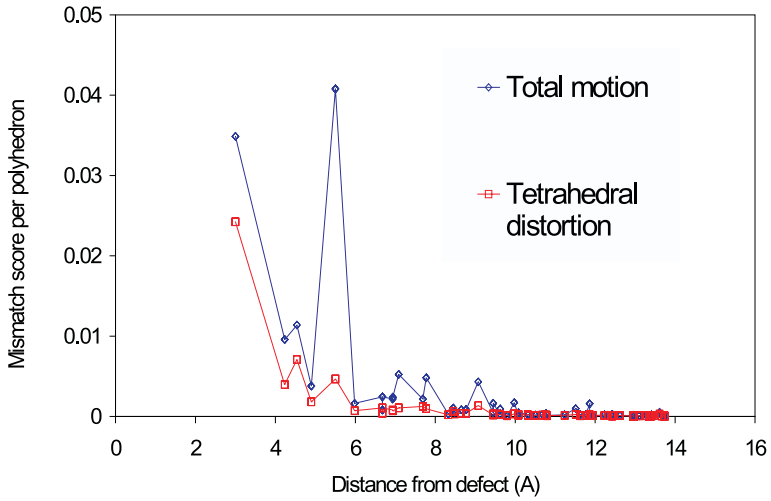

Figure 6. The apparent distortion of the structure due to the presence of the defect (upper line) is largely accommodated by rotational motions of the tetrahedra, leaving a much smaller quantity of actual tetrahedral distortion (lower line). The horizontal axis gives distance from the defect centre in Å; the vertical axis gives the mismatch score per polyhedron in $Å^2$.

uses empirical interatomic potentials, and relaxes the structure around a defect site up to a predefined cut-off. The rest of the crystal is approximated as a polarizable medium.

In this case study we considered the effect of an Al^{3+} substitutional defect on the structure of SiO_2 cordierite. The structure was relaxed out to a radius of 15 Å. We applied our rotor-fitting algorithms to match the polyhedra in the defective structure to the polyhedra in the initial, undistorted structure. The initial mismatch score M_{before} describes the change in the structure due to the defect while the final mismatch score M_{after} indicates actual tetrahedral distortion. The difference between the two is a measure of the degree to which the distortion is accommodated by RUM-like rotations of the polyhedra.

Figure 6 shows the initial and final mismatch scores per polyhedron as a function of distance from the defect centre. Three phenomena are immediately clear. Firstly, the tetrahedra that are nearest neighbours to the defect site are highly distorted by the presence of the defect. Secondly, the next-nearest neighbours to the defect site undergo considerable motion due to the presence of the defect (note the evident peak in the line 'total motion' at just <6 Å), but this motion is largely accounted for by rigid-unit motion of the tetrahedra. Thirdly, the elastic strain in the structure due to the presence of the defect, as represented by the line 'tetrahedral distortion', drops off very rapidly with distance from the defect centre. It appears that the accommodation of the defect by rigid-unit motions of the nearby tetrahedra has the effect of screening the structure at larger distances from the effects of the defect.

Quantitatively, the total-mismatch score over the nearest 268 polyhedra to the defect centre is reduced from 0.55 to 0.21 $Å^2$ by rotations of the polyhedra—an accommodation of just over 60%. Of this residual mismatch, a total of 0.10 $Å^2$ resides on the highly distorted nearest-neighbour tetrahedra—45% of the total residual mismatch. A total of 0.16 $Å^2$, or 72%, resides on polyhedra within 6 Å of the defect centre, while a total of 0.207 $Å^2$, or 97%, resides within 12 Å. Figure 7 gives the displacements of the Si atoms from their initial positions as a result of the defect; these displacements also drop off rapidly with distance from the defect centre.

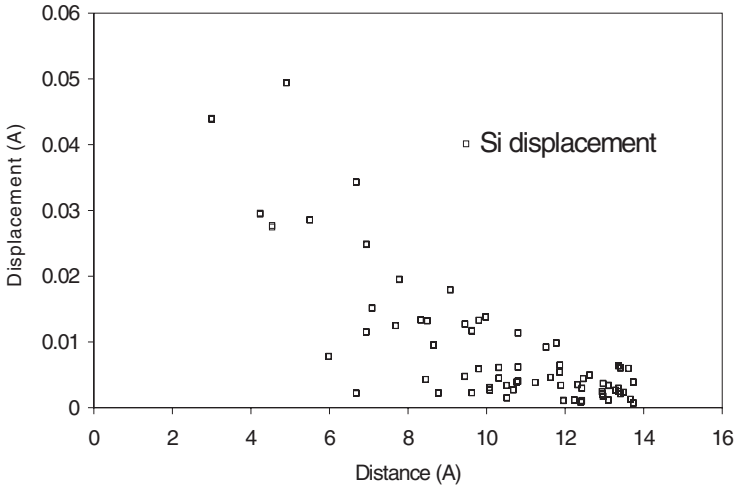

Figure 7. The displacement of the silicon atoms drops off rapidly with distance from the defect centre. Horizontal axis: distance from defect centre in Å; vertical axis: displacement in Å.

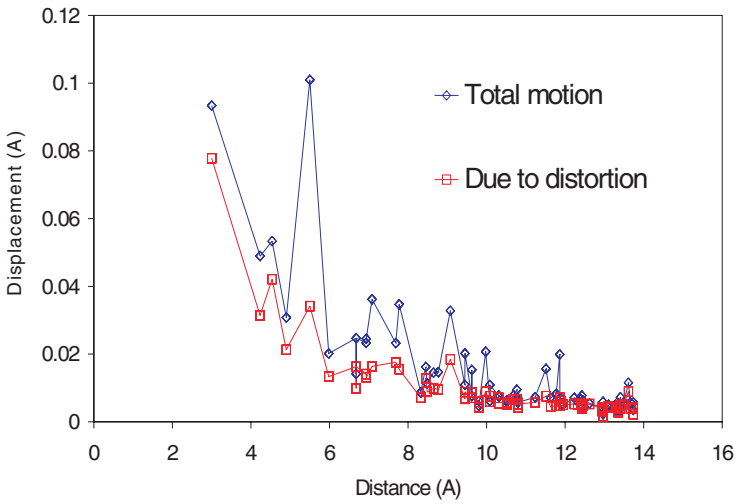

Figure 8. The average motion of the oxygen atoms relative to the silicon atoms also drops off rapidly with distance from the defect centre. It is largely accounted for by rotational motions of the tetrahedra and is of the same order of magnitude as the motions of the silicon atoms. Horizontal axis: distance from defect centre in AA; vertical axis: RMS displacement in Å.

Figure 8 gives the data from figure 6 interpreted as the RMS displacement of oxygen atoms relative to the Si atoms to which they are bonded. The calculation is not difficult as the mismatch score for each polyhedron is simply the sum of the squares of the atomic displacements relative to the Si atom at the centre. These displacements are of a magnitude comparable with the displacements of the Si atoms, and, as we have seen, drop off rapidly with distance from the defect centre and are largely accounted for by rotational motions of the polyhedra.

6. Discussion

In this paper we have introduced a new method for analysing rotations of tetrahedra within crystal structures using the tools of GA, and then used this method to study the rigid-body rotations of tetrahedra in two distinct applications. The first was concerned with the changes in the atomic fluctuations (phonons) in quartz on heating through the phase transition. The GA analysis has shown that the major contribution to the dynamical disorder associated with the phase transition is due to low-energy rigid-unit modes. The analysis has, for the first time, quantified the role of the RUM fluctuations relative to other fluctuations.

The second application has been concerned with incorporation of defects in frameworks of connected tetrahedral sites, and the strain fields that propagate as a result of the defect. The primary finding has been that the significant contribution to the nearest-neighbour interaction arises from deformations of the tetrahedra, but there are large-amplitude atomic displacements for other neighbours that accommodate the strain and which are primarily associated with rigid-tetrahedral rotations.

These examples have been described as illustrative case studies, and more detailed and more general analyses will be given elsewhere. The case studies have shown how the tools based on GA can provide quantitative information

GA is not a commonly taught mathematical system. Most scientists learn vector and tensor algebra, largely for historical reasons, vector algebra being so bound up with the development of electromagnetism. However, GA has proved useful in scientific and engineering applications [21–23], particularly in handling rotations and reflections. Since GA uses bivectors to describe rotations, it avoids the confusing distinction between true vectors and 'axial vectors' with their differing behaviour under reflection. Operations are carried out using the geometric product rather than by matrix operators, which leads to greater mathematical clarity and simplicity. The bivector form for rotations naturally gives a convenient parametrization in terms of the components of the bivector, avoiding any coordinate singularity at the origin.

The algebraic forms describing the rotation (7)–(9) proved convenient for computational use, giving simple routines and a robust and swiftly converging minimization.

Appendix. Mathematical background

A.1. Axioms of GA

GA makes use of a basis set of vectors (not necessarily orthogonal) x_i, whose number is equal to the dimensionality of the vector space, and a geometric product denoted by juxtaposition: ab. This product is distributive: $(a(b+c) = ab+ac)$ and associative: $(a(bc) = (ab)c = abc)$ but not necessarily commutative. The square of any vector is a scalar, which is not required to be positive; however, we will only deal here with Euclidean space in which our basis vectors have positive square.

For two vectors, the product may be decomposed into a symmetric part $a \cdot b = \frac{1}{2}(ab + ba)$ and an antisymmetric part: $a \wedge b = \frac{1}{2}(ab - ba)$. The symmetric part is identical to the usual dot product in vector algebra, being a scalar equal to $|a||b| \cos(\theta)$. However, the antisymmetric part is not a vector cross product, but rather a new object known as a bivector, representing the plane common to the two vectors, as in figure A.1. When we come to deal with rotations in three dimensions, we will see that bivectors act similarly to quaternions. It is conventional not to distinguish vectors in GA by any special type-face.

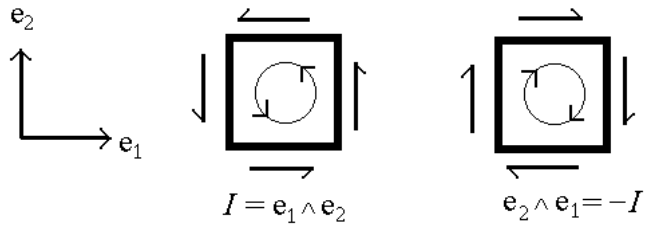

Figure A.1. Formation of a bivector.

We may describe objects in GA according to the number of orthogonal vectors that multiply together to generate them; thus a scalar is a grade 0 object, vectors have grade 1, bivectors have grade 2, and so on. The highest-grade object in the algebra has a grade equal to the dimension of the vector space. All of the objects of the algebra are formed as products of the basis vectors x_i. A general multivector can include objects of all grades. In dealing with rotations we will mostly be concerned with vectors (grade 1) and rotors, which contain objects of even grade. A few examples will suffice to make these ideas clear.

A.2. Two-dimensional GA

GA in two dimensions is easy to grasp as there is a direct analogy to the familiar mathematics of complex numbers. A two-dimensional vector space has a four-dimensional GA, comprising the following objects: $\{1\}$, the scalar; $\{e_1, e_2\}$, the basis vectors; and $\{I\}$, the bivector. We take e_1 and e_2 to be the usual right-handed basis set.

The basis vectors, being orthogonal, have the properties

$$e_1 \cdot e_1 = e_1^2 = 1; \qquad e_2 \cdot e_2 = e_2^2 = 1; \qquad e_1 \cdot e_2 = 0. \tag{A.1}$$

The product e_1e_2 is antisymmetric and gives the bivector $e_1 \wedge e_2 = e_1e_2 = I$. The *reverse* of an object in GA is found by reversing the order of its component vectors, so we may write

$$\tilde{I} = e_2e_1 = -I. \tag{A.2}$$

We can use the associativity of the geometric product to show that I squares to -1, as follows:

$$I^2 = II = e_1e_2e_1e_2 = e_1(e_2e_1)e_2 = e_1(-e_1e_2)e_2 = -e_1^2e_2^2 = -1. \tag{A.3}$$

I is not, however, an imaginary number, but a geometric object of the algebra generated from our basis vectors. Bivectors can be exponentiated just as matrices can, and the property that $I^2 = -1$ means that the usual complex trigonometric identities apply:

$$e^{I\phi} = \cos(\phi) + I\sin(\phi). \tag{A.4}$$

We could represent complex numbers either by a vector in the complex plane, with e_1 representing the real axis:

$$z = ue_1 + ve_2 \tag{A.5}$$

or as a sum of real and bivector parts;

$$z = u + ve_1e_2 = u + vI. \tag{A.6}$$

One form can be converted to the other by left multiplication by e_1. The effect of multiplying our vectors by I depends on the order of multiplication. Multiplication on the left by I gives a clockwise rotation by ninety degrees:

$$Ie_1 = e_1e_2e_1 = -e_1e_1e_2 = -e_2; \qquad Ie_2 = e_1e_2e_2 = e_1; \tag{A.7}$$

while right multiplication by I gives an anticlockwise rotation:

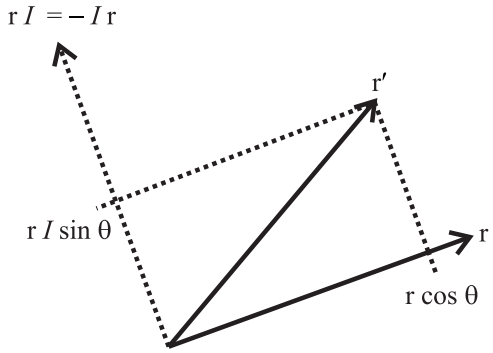

Figure A.2. Rotation of a vector using the bivector I.

$$e_1 I = e_1 e_1 e_2 = e_2; \qquad e_2 I = e_2 e_1 e_2 = -e_1 e_2 e_2 = -e_1. \tag{A.8}$$

We can make use of the effect on vectors of multiplication by the bivector I to represent rotations in the complex plane. An arbitrary vector $x(= x_1 e_1 + x_2 e_2)$ can be rotated anticlockwise in the plane by an angle ϕ by either left multiplication:

$$x' = (\cos(-\phi) + I \sin(-\phi))x = \mathrm{e}^{-I\phi} x, \tag{A.9}$$

or right multiplication:

$$x' = x(\cos(\phi) + I \sin(\phi)) = x\mathrm{e}^{I\phi}. \tag{A.10}$$

We can also perform the rotation using operators on both sides:

$$x' = \mathrm{e}^{-I\phi/2} x \mathrm{e}^{I\phi/2}. \tag{A.11}$$

In this form the operator $R = \exp(-I\phi/2)$ is called a *rotor*. The operator on the right is the reverse of R, as $\tilde{1} = 1$ and $\tilde{I} = -I$, so we can write the rotation as $x' = Rx\tilde{R}$. Rotors are the standard means of expressing a rotation in GA. We note that $R\tilde{R} = 1$, from the definition of the rotor.

A.3. Three-dimensional GA

GA in three dimensions is slightly more complicated than in two. A basis set of three orthonormal vectors generates an algebra of eight objects of various grades: $\{1\}$, the scalar; $\{e_1, e_2, e_3\}$, the basis vectors; $\{e_1e_2, e_2e_3, e_3e_1\}$, three bivectors, often written $\{B_3, B_1, B_2\}$; and $\{e_1e_2e_3\}$, the pseudoscalar (highest-grade object). Both the bivectors and the pseudoscalar square to -1. It is important to note that a bivector commutes with a vector orthogonal to it (example: e_1e_2 commutes with e_3 as $e_1e_2e_3 = -e_1e_3e_2 = e_3e_1e_2$). Multiplication by the pseudoscalar $e_1e_2e_3$ provides the operation of the Hodge dual, relating a bivector to its orthogonal vector.

A general bivector can contain components of all three basis bivectors $\{B_1, B_2, B_3\}$, representing a plane. It can be visualized as the outer product of two vectors in the plane—for example, the bivector $e_1e_2+e_2e_3$ can be written as $(e_1-e_3)\wedge e_2$, that is, the plane containing the vectors $(e_1 - e_3)$ and e_2. Or, in this three-dimensional case, we can apply the Hodge dual and find the vector orthogonal to the bivector; so a general bivector $B = B_x e_2e_3 + B_y e_3e_1 + B_z e_1e_2$ would be orthogonal to the vector $b = b_x e_1 + b_y e_2 + b_z e_3$.

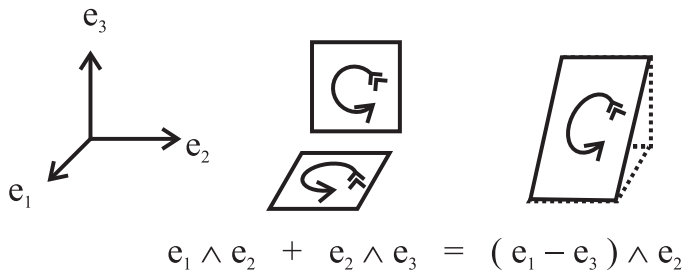

Figure A.3. Addition of bivectors.

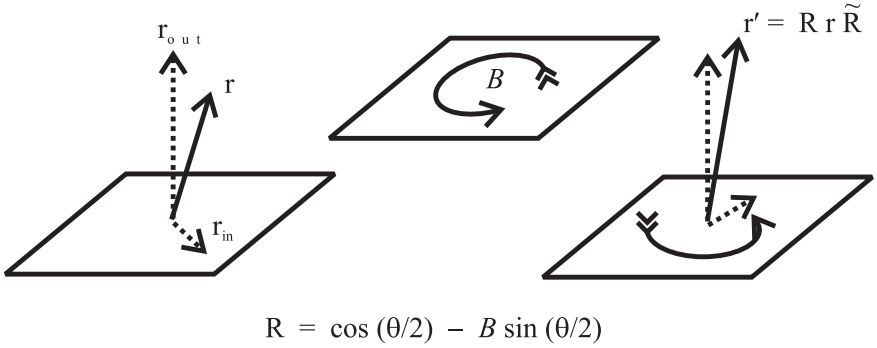

Figure A.4. The rotor operator.

A.4. Rotor operator

In three dimensions we are used to describing a rotation in terms of the axis about which it occurs, for example by means of an axial vector. In GA this idea is considered misleading. We saw in the two-dimensional case how rotations could be described in a plane. In GA we use exactly the same description, whatever the dimension of the space; the rotation is described by its magnitude and by the plane in which it occurs. The plane can be described by a bivector (grade-2 object) made up of some combination of the basis bivectors B_i; the vector normal to this plane, which can be found via the Hodge dual, would be the rotation axis in the conventional picture. So for example a rotation in the plane $\hat{B} = \hat{B}_x e_2 e_3 + \hat{B}_y e_3 e_1 + \hat{B}_z e_1 e_2$ would be described as rotation about the axis $\hat{b} = \hat{b}_x e_1 + \hat{b}_y e_2 + \hat{b}_z e_3$ in vector algebra.

The two-sided rotor operator which we met in the two-dimensional case can also be used in three dimensions. The plane of the rotation is described by a unit bivector $\hat{B}$ ($B^2 = -1$; $B\tilde{B} = 1$). Any vector x can be decomposed into parts perpendicular to the plane of $\hat{B}$, x_{out}, and within the plane, x_{in}. The part lying within the plane is rotated, just as in the two-dimensional case. The part perpendicular to the plane, however, commutes with both the scalar and the bivector $\hat{B}$, and therefore commutes with R. As we noted before, $R\tilde{R} = 1$, and so x_{out} is unaffected by the rotor operator:

$$Rx_{\text{out}}\tilde{R} = x_{\text{out}}R\tilde{R} = x_{\text{out}}. \tag{A.12}$$

Since the rotor operator is a function of the half-angle $\phi/2$ rather than of ϕ, an arbitrary rotation can be described in terms of its plane and an angle $\phi/2$ between zero and $\pi/2$ radians. This is convenient when we write the expansion $R = \cos(\phi/2) - \hat{B}\sin(\phi/2)$, as the sine and cosine terms are always positive. The rotor is illustrated in figure A.4.

The conventional representation of rotors in exponential or trigonometric form is well suited to formal work. However, in this work we have, for the sake of computational convenience, used the following algebraic form:

$$R = X - \tfrac{1}{2}(B_x e_2 e_3 + B_y e_3 e_1 + B_z e_1 e_2) = X - B/2. \tag{A.13}$$

In this form the $B_n e_j e_k$ terms form a bivector B, defining the plane of the rotation. Comparison with the trigonometric form gives the magnitude of B as

$$|B| = \sqrt{B_x^2 + B_y^2 + B_z^2} = 2\sin\left(\frac{\phi}{2}\right), \tag{A.14}$$

so for small angles, $|B| \simeq \phi$. The term X is equal to $\cos(\phi/2)$ and is given by

$$X = \sqrt{\left(1 - \tfrac{1}{4}(B_x^2 + B_y^2 + B_z^2)\right)}. \tag{A.15}$$

The case $B = 0$ is the identity operation; $R(0) = 1$.

References

[1] Hammonds K D, Dove M T, Giddy A P, Heine V and Winkler B 1996 Rigid unit phonon modes and structural phase transitions in framework silicates *Am. Mineral.* **81** 1057–79

[2] Heine V, Welche P R L and Dove M T 1999 Geometric origin and theory of negative thermal expansion in framework structures *J. Am. Ceram. Soc.* **82** 1793–802

[3] Welche P R L, Heine V and Dove M T 1998 Negative thermal expansion in β-quartz *Phys. Chem. Minerals* **26** 63–77

[4] Giddy A P, Dove M T, Pawley G S and Heine V 1993 The determination of rigid unit modes as potential soft modes for displacive phase transitions in framework crystal structures *Acta Crystallogr.* A **49** 697–703

[5] Dove M T, Trachenko K O, Tucker M G and Keen D A 2000 Rigid unit modes in framework structures: theory, experiment and applications *Rev. Mineral. Geochem.* **39** 1–33

[6] Gull S F, Lasenby A N and Doran C J L 1993 Imaginary numbers are not real—the geometric algebra of spacetime *Found. Phys.* **23** 1175–201

[7] Swainson I P and Dove M T 1993 Low-frequency floppy modes in β-cristobalite *Phys. Rev. Lett.* **71** 193–6

[8] Vallade M, Berge B and Dolino G 1992 Origin of the incommensurate phase of quartz. 2. Interpretation of inelastic neutron-scattering data *J. Physique* I **2** 1481–95

[9] Hammonds K D, Dove M T, Giddy A P and Heine V 1994 CRUSH: a Fortran program for the analysis of the rigid unit mode spectrum of a framework structure *Am. Mineral.* **79** 1207–9

[10] Palin E J, Trachenko K O and Dove M T 2002 Computer simulation study of low-energy excitations in aluminosilicate glasses *J. Phys.: Condens. Matter* submitted

[11] Trachenko K, Dove M T, Hammonds K D, Harris M J and Heine V 1998 Low-energy dynamics and tetrahedral reorientations in silica glass *Phys. Rev. Lett.* **81** 3431–4

[12] McGreevy R L and Pusztai L 1988 Reverse Monte Carlo simulation: a new technique for the determination of disordered structures *Mol. Simul.* **1** 359–67

[13] McGreevy R L 1995 RMC—progress, problems and prospects *Nucl. Instrum. Methods* A **354** 1–16

[14] Tucker M G, Dove M T and Keen D A 2001 Application of the reverse Monte Carlo method to crystalline materials *J. Appl. Crystallogr.* **34** 630–8

[15] Tucker M G, Keen D A and Dove M T 2001 A detailed structural characterization of quartz on heating through the α–*beta* phase transition *Mineral. Mag.* **65** 489–507

[16] Dove M T, Thayaparam S, Heine V and Hammonds K D 1996 The phenomenon of low Al/Si ordering temperatures in aluminosilicate framework structures *Am. Mineral.* **81** 349–62

[17] Bosenick A, Dove M T, Myers E R, Palin E J, Sainz-Diaz C I, Guiton B, Warren M C, Craig M S and Redfern S A T 2001 Computational methods for the study of energies of cation distributions: applications to cation-ordering phase transitions and solid solutions *Mineral. Mag.* **65** 193–219

[18] Winkler B, Dove M T and Leslie M 1991 Static lattice energy minimization and lattice dynamics calculations on minerals using three-body potentials *Am. Mineral.* **76** 313–31

[19] Gale J D 1997 GULP: a computer program for the symmetry-adapted simulation of solids *J. Chem. Soc. Faraday Trans.* **93** 629–37

[20] Lasenby A N, Doran C J L and Gull S F 1996 Lectures in geometric algebra *Clifford (Geometric) Algebras with Applications to Physics, Mathematics and Engineering* ed W E Baylis (Cambridge, MA: Birkhäuser)
[21] Lasenby J 1996 Geometric algebra: applications in engineering *Clifford (Geometric) Algebras with Applications to Physics, Mathematics and Engineering* ed W E Baylis (Cambridge, MA: Birkhäuser)
[22] Lasenby A N and Lasenby J 2000 Applications of geometric algebra in physics and links with engineering *Geometric Algebra: a Geometric Approach to Computer Vision, Neural and Quantum Computing, Robotics and Engineering* ed E Bayro and G Sobczyk (Basle: Birkhäuser)
[23] Lasenby J, Lasenby A N and Doran C J L 2000 A unified mathematical language for physics and engineering in the 21st century *Phil. Trans. R. Soc.* A **358** 21–39
[24] The Geometric Algebra Research Group home-page. http://www.mrao.cam.ac.uk/ clifford/
[25] Dove M T, Keen D A, Hannon A C and Swainson I P 1997 Direct measurement of the Si–O bond length and orientational disorder in β-cristobalite *Phys. Chem. Minerals* **24** 311–7
[26] Gambhir M, Dove M T and Heine V 1999 Rigid unit modes and dynamic disorder: SiO_2 cristobalite and quartz *Phys. Chem. Minerals* **26** 484–95
[27] Swainson I P and Dove M T 1995 Molecular dynamics simulation of α- and β-cristobalite *J. Phys.: Condens. Matter* **7** 1771—88
[28] Tucker M G, Squires M D, Dove M T and Keen D A 2001 Dynamic structural disorder in cristobalite: neutron total scattering measurement and reverse Monte Carlo modelling *J. Phys.: Condens. Matter* **13** 403–23